Structure of a closed form of human malic enzyme and implications for catalytic mechanism

Zhiru Yang[1], Daniel L. Floyd[1], Gerhard Loeber[2] and Liang Tong[1]

Malic enzymes are widely distributed in nature and have many biological functions. The crystal structure of human mitochondrial NAD(P)$^+$-dependent malic enzyme in a quaternary complex with NAD$^+$, Mn^{++} and oxalate has been determined at 2.2 Å resolution. The structures of the quaternary complex with NAD$^+$, Mg^{++}, tartronate or ketomalonate have been determined at 2.6 Å resolution. The structures show the enzyme in a closed form in these complexes and reveal the binding modes of the cation and the inhibitors. The divalent cation is coordinated in an octahedral fashion by six ligating oxygens, two from the substrate/inhibitor, three from Glu 255, Asp 256 and Asp 279 of the enzyme, and one from a water molecule. The structural information has significant implications for the catalytic mechanism of malic enzymes and identifies Tyr 112 and Lys 183 as possible catalytic residues. Changes in tetramer organization of the enzyme are also observed in these complexes, which might be relevant for its cooperative behavior and allosteric control.

Malic enzyme (ME) catalyzes the oxidative decarboxylation of L-malate to pyruvate with the concomitant reduction of the cofactor NAD$^+$ or NADP$^+$ (refs 1–5). The catalysis of this reaction, NAD(P)$^+$ + L-malate $\rightleftharpoons$ NAD(P)H + pyruvate + CO_2, also requires divalent cations (Mg^{++} or Mn^{++}). Malic enzymes have been found in most living organisms, from bacteria to humans, and their amino acid sequences are highly conserved across these organisms[6], suggesting that they may have important biological functions[5]. In mammals, three isoforms of ME have been identified[6] — a cytosolic NADP$^+$-dependent ME (c-NADP-ME), a mitochondrial NADP$^+$-dependent ME (m-NADP-ME), and a mitochondrial NAD(P)$^+$-dependent ME (m-NAD-ME). m-NAD-ME can use both NAD$^+$ and NADP$^+$ as the cofactor (dual specificity), but prefers NAD$^+$ under physiological conditions[1]. The m-NAD-ME isoform may have an important role in the metabolism of glutamine for energy production in rapidly proliferating tissues and tumors[1,7,8]. A metabolic role for m-NAD-ME is consistent with its cooperative behavior with respect to the substrate malate and allosteric regulation[5], with fumarate as an activator and ATP as an inhibitor[9], which is unique among malic enzymes.

The amino acid sequences of ME contain two dinucleotide binding signature motifs, GXGXXG/A (ref. 10), corresponding to 168-GLGDLG-173 and 311-GAGEAA-316 in m-NAD-ME. Besides these two motifs, ME does not show recognizable amino acid sequence homology to other proteins, such as the dehydrogenases and the decarboxylases. We recently reported the crystal structure of m-NAD-ME in a binary complex with NAD$^+$ at 2.1 Å resolution[5]. The structure established malic enzymes as a new class of oxidative decarboxylases, identified Glu 255, Asp 256, Asp 279 as possible ligands of the divalent cation, revealed the binding site for the NAD$^+$ molecule in the active site, and revealed the organization of the tetramer of the enzyme. The binding site for a second NAD$^+$ molecule (exo site) in m-NAD-ME may correspond to that for the allosteric inhibitor, ATP. The structure of the m-NAD-ME monomer can be divided into four domains, A–D. Domains A (residues 23–130) and D (539–573) are mostly involved in dimer and tetramer formation, whereas domains B (131–277 and 467–538) and C (278–466), and several residues from domain A, are responsible for the catalysis by the enzyme.

However, it is apparent from the structure of the binary complex that the enzyme is in an open form[5]. The binding modes of the divalent cation and of the substrates or the substrate-analog inhibitors, the conformation of the closed form, and the catalytic mechanism of the enzyme remain to be elucidated. The closed form of the enzyme is expected to bind the substrate/cation and carry out catalysis. We report here crystal structures of human m-NAD-ME in a closed form, in quaternary complexes with NAD$^+$, the divalent cation Mn^{++} or Mg^{++}, and the substrate-analog inhibitors oxalate ($^-$OOCCOO$^-$, a mimic of the enol-pyruvate intermediate), tartronate ($^-$OOCC(HOH)COO$^-$) or ketomalonate ($^-$OOCCOCOO$^-$). There are large differences both in the conformation of the m-NAD-ME monomer and in the organization of the tetramer between the open form reported earlier and the closed form observed here.

Overall structure

The structure of human mitochondrial NAD(P)$^+$-dependent malic enzyme (m-NAD-ME) in a quaternary complex with NAD$^+$, Mn^{++} and oxalate (OXL) has been determined at 2.2 Å resolution (Table 1). The current atomic model contains residues 21–573 for each monomer of the tetramer in the asymmetric unit (Fig. 1*a*). As was observed with the NAD$^+$ binary complex[5], two NAD$^+$ molecules are associated with each monomer of m-NAD-ME in the quaternary complex. The NAD$^+$ molecule at the exo site has similar interactions with the protein as those in the binary complex[5]. While the crystallization solution also contained 5 mM fumarate, the allosteric activator of

[1]Department of Biological Sciences, Columbia University, New York, New York 10027, USA. [2]Boehringer Ingelheim Austria Research and Development, Dr. Boehringer-Gasse 5-11, A-1121 Vienna, Austria.

Correspondence should be addressed to L.T. *email: tong@como.bio.columbia.edu*

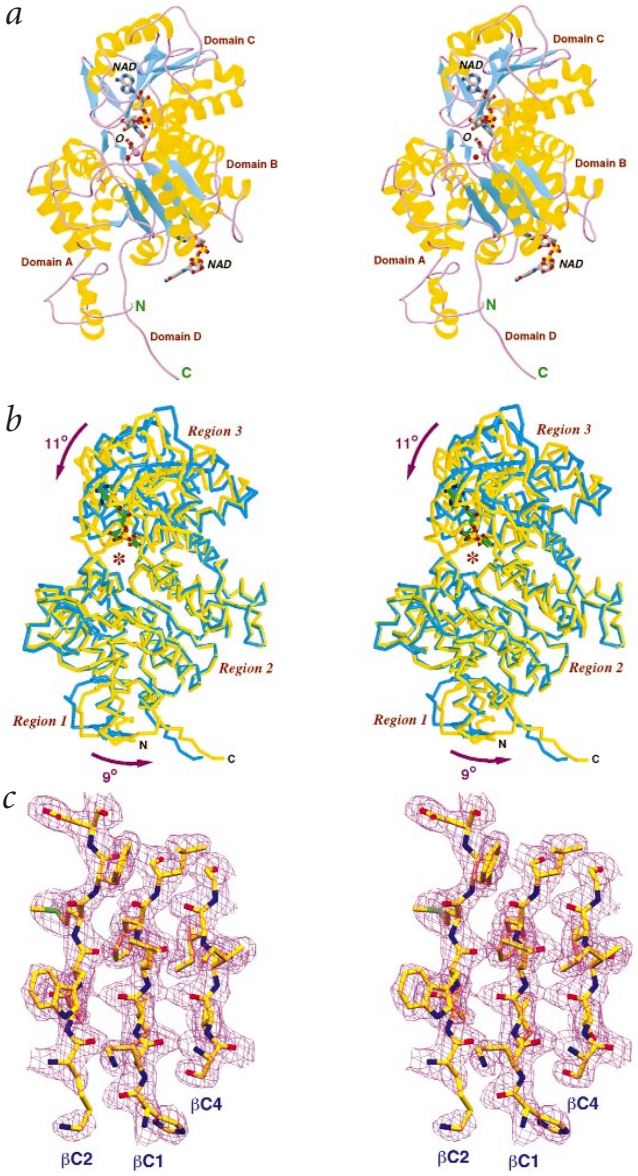

Fig. 1 Overall structure of human malic enzyme. ***a***, Schematic drawing[29] of the structure of m-NAD-ME in complex with NAD^+, Mn^{++} and oxalate. The β-strands are shown in cyan, α helices in yellow, and the connecting loops in purple. The four domains of the structure are labeled. The two NAD^+ molecules bound to the enzyme and the oxalate molecule in the active site are shown as stick models, colored according to atom types (carbon gray, oxygen red, nitrogen blue, and phosphorus yellow). The oxalate molecule is labeled with the letter O. The manganese ion and its ligating water molecule are shown as pink and red spheres, respectively. ***b***, Overlap[30] of the Cα traces of m-NAD-ME in open (binary complex with NAD^+, shown in cyan) and closed (quaternary complex with NAD^+, Mn^{++} and oxalate, in yellow) forms, with region 2 of the two structures in superposition. The NAD^+ molecule in the active site is shown as a stick model. The active site is marked with a red star. The three rigid body regions are labeled. ***c***, Final $2F_o$ - F_c electron density map at 2.2 Å resolution for some of the β-sheet residues in domain C in the oxalate complex. The contour level is at 1 σ. Figures were generated using RIBBONS[29] and GRASP[30].

this enzyme, it could not be located in the electron density map and is probably not bound to the enzyme in the crystal. There is a cluster of six Arg residues at the dimer interface, including Arg 91, Arg 128, Arg 129 and their symmetry-mates. The binding site for fumarate, which has an internal two-fold symmetry, could be located here. The four monomers of the m-NAD-ME tetramer have very similar conformations. The root mean square (r.m.s.) deviation between the 553 equivalent Cα positions of any pair of monomers is ~0.2 Å. The tetramer maintains almost perfect 222 symmetry, so each monomer has the same environment in the tetramer.

The structure of m-NAD-ME in a quaternary complex with NAD^+, Mg^{++} and ketomalonate has been determined at 2.6 Å resolution (Table 1). This crystal is isomorphous to that of the OXL complex, and the monomer conformation and the tetramer organization in this complex are essentially the same as in the OXL complex.

The structure of m-NAD-ME in a quaternary complex with NAD^+, Mg^{++} and tartronate has been determined at 2.6 Å resolution (Table 1). This crystal was non-isomorphic in unit cell parameters compared to those of the OXL or ketomalonate complex (Table 1). However, the conformation of the monomers in this complex is essentially the same as that of the monomers in the OXL (or ketomalonate) complex. The r.m.s. deviation between the 553 equivalent Cα positions of any pair of monomers from the two structures is ~0.3 Å. The organization of the dimer and tetramer of the enzyme is slightly different between the two structures, with an r.m.s. deviation of 0.6 Å when the 2,212 Cα atoms of the two tetramers are superimposed.

A closed form of the enzyme

There are significant differences in the conformation of the monomer in the quaternary complex observed here compared to that in the binary NAD^+ complex[5] (Fig. 1*b*). A superposition of 539 equivalent Cα (lying within 3 Å) from monomers in the two complexes produced an r.m.s. distance of 1.4 Å. In the current structure, domains B and C have moved closer together, forming a tight fit around the bound cation and the substrate-analog inhibitor (Fig. 1). Therefore, the quaternary complex represents a closed form of the m-NAD-ME enzyme, whereas the binary complex with NAD^+ is an open form of the enzyme. Furthermore, in the binary complex, residues in domain C exhibit conformational disorder as evidenced by their weaker electron density[5]. In the current structure, the conformation of these residues are stabilized in the closed form and they have well-defined electron density (Fig. 1*c*).

The conformational difference is mostly due to relative rigid body movements among three regions of the structure. Region 3 contains residues in domain C (280–465), together with a short stretch from domain B (501–516, helix αB7). The r.m.s. deviation between these 202 Cα atoms of the two structures is 0.5 Å. The short stretch from domain B (501–516) helps close the hydrophobic core of domain C, burying the side chains of four conserved residues, Leu 507, Gly 510, Leu 512 and Tyr 513. The superposition also brings the ADP moiety of the NAD^+ molecule in the active site into overlap, confirming that NAD^+ binding is mediated by the Rossmann fold in domain C. The positions of the nicotinamide and the ribose moieties in NAD^+ are slightly different in the two structures, with a distance of 0.9 Å between the two C4 atoms in the nicotinamide ring. With residues in region 3 in overlap, a rotation of 10.6° is required to bring region 2 into superposition, which includes most of the residues in domain B and some in domains A and D (76–279, 467–500 and 517–560). The r.m.s. deviation for 282 Cα atoms in region 2 is 0.6 Å. This superposition shifted residues near the active site (Leu 167, Cys 120, Ile 179, Arg 165) by ~4 Å. These residues in their new positions help define the closed form of the enzyme. Region 1

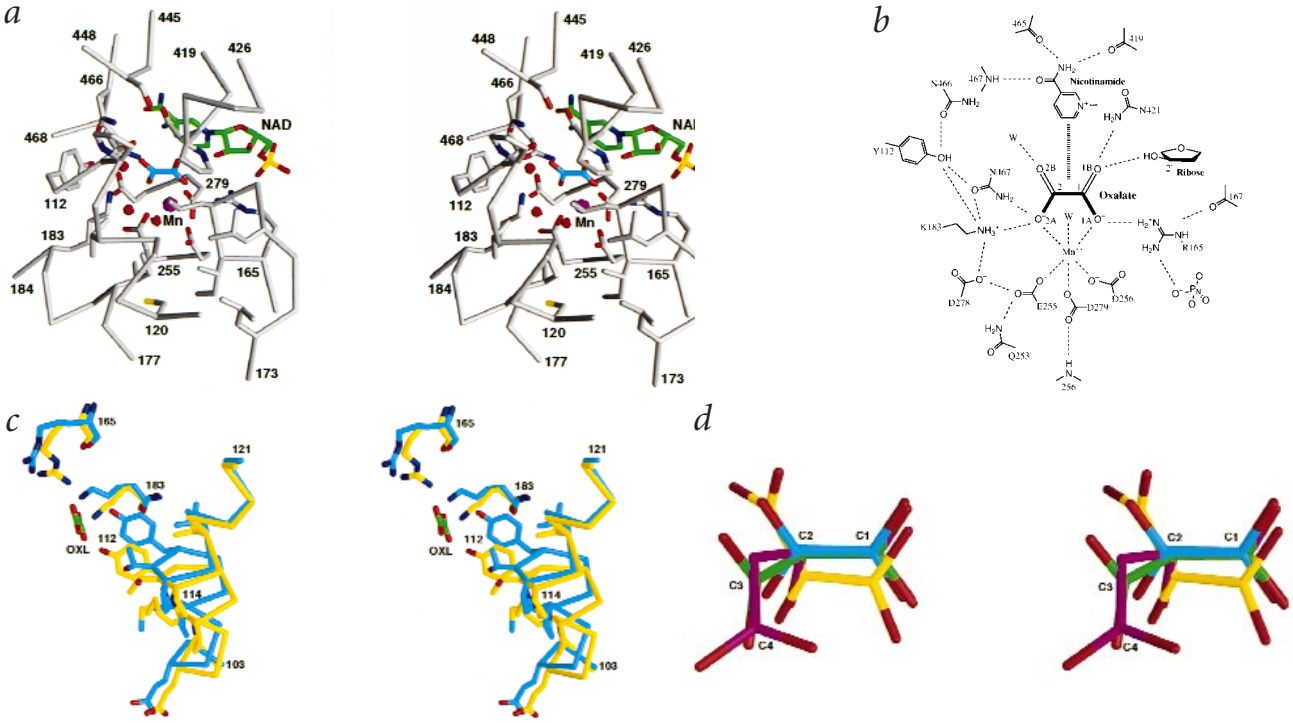

Fig. 2. The active site of human malic enzyme. ***a***, Stereo diagram showing the active site of m-NAD-ME. Protein residues are shown with the carbon atoms in gray, the NAD^+ cofactor with the carbon atoms in green, and the oxalate with the carbon atoms in cyan. The manganese ion is shown as a purple sphere, and solvent molecules are shown as small red spheres. ***b***, Schematic drawing of the Mn^{++}–oxalate binding site. The atoms of the oxalate molecule are labeled. Water molecules are shown as W. The potential π-π interaction between the oxalate and nicotinamide is also indicated. ***c***, Conformational differences between the open (shown in cyan for carbon atoms) and closed (in yellow) forms near the active site, for residues 103–121 (helix αA6), 165 and 183. ***d***, The binding modes of oxalate (with carbon atoms in cyan), ketomalonate (yellow), and tartronate (green). A proposed binding mode for the substrate malate is also indicated (in purple for carbon atoms).

contains residues from domains A and D (23–75 and 561–573). With region 2 in overlap, a further rotation of 9.2° is needed to bring this region into superposition, giving an r.m.s. deviation of 0.7 Å for the 66 Cα atoms. The position of Trp 572 near the C-terminus is shifted by more than 6 Å by this superposition.

Within the framework of rigid body movements among the three regions, there are local conformational differences in each of the regions as well. These local differences are reflected by the 0.6 Å r.m.s. deviation between equivalent Cα atoms in the three regions, which is higher than the expected errors in the atomic coordinates. Some of these differences are important for substrate binding and tetramer reorganization and is discussed below.

The binding modes of Mn^{++} and oxalate

The active site of the enzyme is located at the interface between domains B and C in each monomer, together with contributions from a few residues of domain A[5] (Fig. 1*a*). The divalent cation Mn^{++} is bound deep in this cleft, with six oxygen atoms as ligands arranged in an octahedral fashion (Fig. 2). The side chain carboxylate groups of Glu 255, Asp 256 and Asp 279 each contribute one ligand to the cation, confirming predictions based on the NAD^+ binary complex[5]. Asp 279 has also been identified as a cation ligand based on Fe-ascorbate affinity cleavage and site-specific mutagenesis studies on the pigeon liver ME[11,12]. Oxalate contributes two ligands, one from each of its two carboxylate groups. The sixth ligand is a water molecule (Fig. 2*b*). The average distance between Mn^{++} and the six oxygen ligands is 2.3 Å. In addition to ligating the cation, residues Glu 255, Asp 256 and Asp 279 are involved in a large network of hydrogen bonding interactions (Fig. 2*b*). For example, the other carboxylate oxygen atom of Asp 279 is hydrogen bonded to the main chain amide of Asp 256, thereby connecting the two sets of cation ligands together.

The oxalate molecule is bound with its plane parallel to and ~3.5 Å from that of the nicotinamide ring of NAD^+, suggesting possible π–π interactions (Fig. 2*b*). There is a large network of hydrogen bonding and ionic interactions near the oxalate molecule. The C1 carboxylate group in oxalate shows mono-dentate ionic interactions with the side chain guanidinium group of Arg 165, using the same oxygen atom (O1A) that is ligated to the cation. The side chain of Arg 165 also interacts with a phosphate group of NAD^+. The other oxygen atom of the C1 carboxylate (O1B) is within hydrogen bonding distance to the side chain amide of Asn 421 and the 2'-hydroxyl of the nicotinamide ribose. For the C2 carboxylate, the oxygen atom that is ligated to the cation (O2A) forms ionic interactions with the side chain of Lys 183, as well as hydrogen bonding interactions with the side chain amide of Asn 467 (Fig. 2*b*). The other oxygen atom (O2B) points towards a small cavity in the protein, and is hydrogen bonded to a solvent molecule in this region.

The shape of the active site is determined by the side chains of many residues, including Tyr 112 and Val 116 from domain A, Ile 179, Ile 166 and Leu 167 from domain B, Asn 421 and Ser 447 from domain C. Pro 114 and Pro 422, both in the *cis* conformation, close the top of the binding pocket and help to shield the oxalate molecule from the bulk solvent in the closed form (Fig. 2*a*). Most of these residues are highly conserved in the malic enzymes. The side chain of Cys 120 is about 13 Å away from the oxalate molecule (Fig. 2*a*), suggesting that the inhibitory effect of its modification on malate binding[13] is indirect. Chemical modifi-

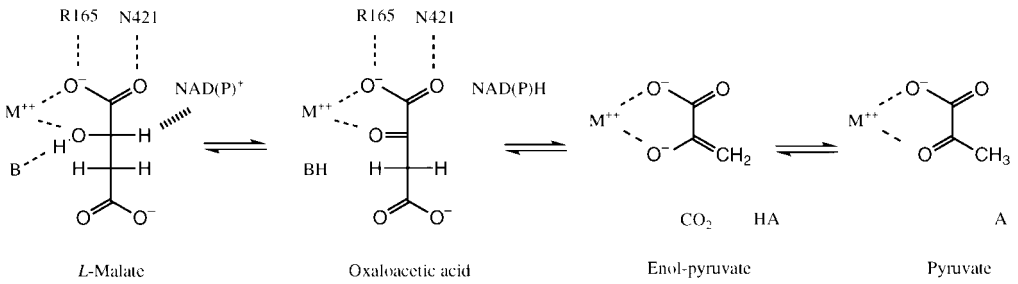

Fig. 3. A possible catalytic mechanism for malic enzymes. B represents the general base and HA the general acid that are required for this mechanism. Oxalate is a mimic for the enol-pyruvate intermediate in this mechanism.

cation of one Arg residue in pigeon and maize ME eliminated the binding of malate without affecting the binding of the $NADP^+$ cofactor[14,15]. The current structure suggests that this Arg residue may correspond to Arg 165. It is involved in binding the C1 carboxylate of oxalate, and is conserved in pigeon and maize ME. However, this residue is not strictly conserved among all malic enzymes.

In addition to the rigid body movements that produced the closed form of the enzyme, several residues near the active site have local conformational differences between the quaternary and the binary complexes. Residues 105–115 of helix αA6, 165–171 of the highly conserved TDGERILGLGDLG motif, and the side chains of Lys 183 and Asn 467 showed the largest differences (Fig. 2*c*). The position of the Lys 183 side chain in the quaternary complex, which forms ionic interactions with oxalate, is in steric clash with that of Tyr 112 in the open form, suggesting that these conformational changes may be triggered by the binding of substrates/inhibitors (Fig. 2*c*).

The binding modes of ketomalonate and tartronate

The observed electron density for both ketomalonate and tartronate are smaller than would be expected based on their chemical structures, suggesting either disorder or partial occupancy in the crystal. This possibly introduces some uncertainty in the models of the bound conformations of these compounds (Fig. 2*d*). The C1 and C2 atoms of OXL were modeled to correspond to the C1 and C2 atoms of ketomalonate and tartronate, respectively. This left the C3 carboxylate groups in both ketomalonate and tartronate in very weak electron density, although this also placed the C3 groups in the cavity that is observed in the OXL complex. The interactions of ketomalonate and tartronate with the divalent cation and the enzyme in this binding mode are generally similar to that observed for the OXL complex. An alternative binding orientation, where the C1 and C2 atoms of tartronate correspond to the C2 and C1 atoms of oxalate, respectively, would position the C3 carboxylate group too close to Leu 167 of the enzyme and is therefore unlikely.

Implications for the catalytic mechanism

Noting the presence of a cavity near the C2 atom of oxalate and the lack of extra space near the C1 atom, we modeled the C1 and C2 atoms of the substrate malate to correspond to the C1 and C2 atoms of oxalate (Fig. 2*d*). In this model, the C4 carboxylate group of malate is placed in the cavity and could interact with the side chain of Lys 183. The proton on the C2 atom of malate points towards the C4 atom of the nicotinamide ring with a distance of ~2.7 Å. This proposed binding mode for malate can explain both the proton transfer between malate and NAD^+ and the stereospecificity of ME for L-malate, as D-malate cannot bind in the same way as L-malate because of a steric clash between the C2 hydroxyl and the nicotinamide. Furthermore, this model predicts a proton transfer to the A face of the nicotinamide ring, in agreement with experimental observations[16]. The orientation of the malate molecule relative to the nicotinamide-ribose in this binding mode, with the C4 atom further away from the ribose than the C1 atom, is opposite that in malate dehydrogenase[17], where the C4 atom is closer to the ribose.

The catalysis by malic enzymes generally proceeds in two steps — dehydrogenation of malate to produce oxaloacetate, and then decarboxylation to produce pyruvate[4]. A possible mechanism for the catalysis that is consistent with the current structural information is shown in Fig. 3. The observed binding mode of the cation places it at the optimal position to catalyze both steps of the reaction, polarizing the C2 hydroxyl of malate for dehydrogenation and stabilizing the C2 enolic oxygen for decarboxylation. Previous studies had indicated a water-mediated interaction between the cation and the substrate[18,19]. This is, however, inconsistent with the current structural information. The lack of space in the active site near the cation makes a water-mediated interaction unlikely.

For the proposed mechanism, a general base is required to extract the C2 hydroxyl proton in the dehydrogenation step, and a general acid is required to protonate the enol-pyruvate product of decarboxylation. Of the residues located near the O2A atom of oxalate (Fig. 2*b*), Tyr 112 and Lys 183 are likely candidates for the catalytic residues. Lys 183 is strictly conserved among the malic enzymes, while Tyr 112 is conserved except in one plant enzyme. Moreover, a Lys and a Tyr residue have also been found in the active site of isocitrate dehydrogenase (IDH), a different class of oxidative dehydrogenases[5,20]. Mutation of the Tyr residue to a Phe in IDH severely reduced the rate of the dehydrogenation step, whereas mutation of Lys to Met abolished the decarboxylation reaction[21]. Lys 183 and Tyr 112 may have similar functions in the catalysis by m-NAD-ME and mutagenesis studies are underway to confirm this. The structural basis for the catalytic role of the Tyr residue in the dehydrogenation reaction remains to be established, given that the C2 hydroxyl of the substrates and the side chain hydroxyl of the Tyr residue are separated by a distance of more than 4.5 Å in both ME and IDH.

Besides Lys 183 and Tyr 112, several other highly conserved residues are located near the C2 carboxylate of OXL, including Asp 278, Asn 466, and Asn 467. These residues are part of the hydrogen bonding network that also include Lys 183 and Tyr 112 (Fig. 2*b*). The side chain of Asp 278 is in direct interaction with that of Lys 183 and is completely shielded from the solvent. Therefore, Asp 278, Asn 466 and Asn 467 may also have important roles in the catalysis by malic enzymes.

The three-dimensional structures of ME and IDH bear no relationship. The active site in IDH is located at the interface of a

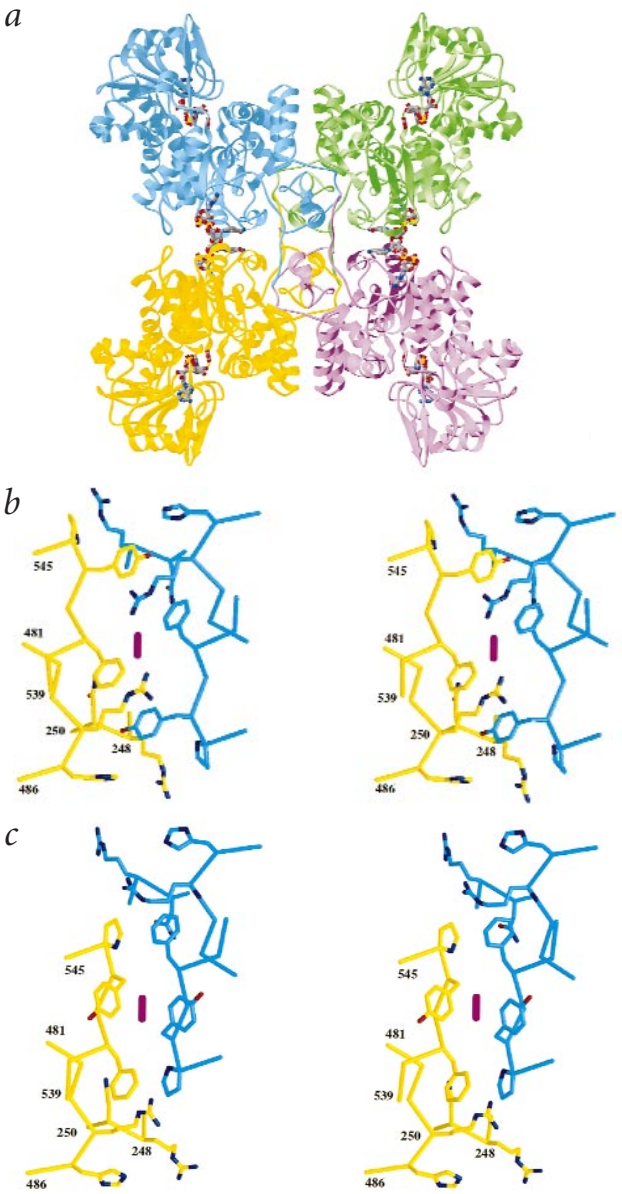

Fig. 4. The tetramer of human malic enzyme. ***a***, Schematic drawing of the tetramer of m-NAD-ME in the closed form. The monomers are colored in green, cyan, yellow and purple, respectively. The bound NAD^+ and oxalate molecules are shown in stick representation. ***b***, Stereo diagram showing part of the tetramer interface in the oxalate complex involving residues 541–544. The carbon atoms of the two monomers at this interface are shown in yellow and cyan, respectively. The location of the two-fold axis is indicated by the purple bar. ***c***, The tetramer interface in the NAD^+ binary complex, for the same residues as those in (*b*). There is a large change in the relative positions of the two monomers in this region, together with a change in the side chain conformation for Tyr 543.

dimer, with the Lys and Tyr residues coming from different monomers of the dimer[20,21]. In comparison, the active site in ME is located within the monomer, about 30 Å away from the interfaces of the tetramer[5]. Moreover, the substrates of the two enzymes have opposite stereochemistry at the C2 position, with the C2 hydroxyl in isocitrate corresponding to that in D-malate. Nonetheless, the proposed catalytic mechanism and identity of the catalytic residues show remarkable similarity between the two enzymes. This suggests that the mechanisms of ME and IDH may represent an example of convergent evolution for metal-mediated oxidative decarboxylases.

A unique property of m-NAD-ME is its dual specificity with respect to the dinucleotide cofactor. This enzyme contains an Asp residue (Asp 345) near the end of strand β2 of the Rossmann fold in domain C, and would normally indicate NAD^+ specificity — the Asp side chain recognizes the hydroxyls on the ribose and can not tolerate the negatively charged 2'-phosphate group of $NADP^+$ (ref. 22). In the structure of m-NAD-ME, the side chain of this Asp residue points away from the ribose, forming ionic interactions with Arg 354. The Asp residue is strictly conserved, and the Arg residue is mostly conserved among malic enzymes. The relevance of this ionic interaction to the dual specificity of m-NAD-ME will require further studies.

A change in tetramer organization

There are significant differences in the organization of the tetramer in the quaternary complex with OXL and the binary complex with NAD^+. To analyze these differences, we first superimposed the equivalent two-fold symmetry axes of the two tetramers. We then independently superimposed the three individual regions that show rigid body movements between the two structures. A rotation of 5° is needed to bring equivalent residues in region 1 of the two structures into overlap. This suggests a reorganization of the tetramer, as residues in this region are at the dimer and tetramer interfaces. An independent rotation of 6° is needed to bring residues in region 2 into overlap. Residues 214–219 and 541–544 in this region show local conformational differences. The former is located at the dimer interface, and the latter is at the tetramer interface. For region 3, a rotation of 13° is needed, due to the closed conformation of the OXL complex. However, it appears that the closure of the active site may occur independently of the reorganization of the tetramer. In the structure of m-NAD-ME–NAD^+–Lu^{3+} ternary complex, a reorganization of the tetramer was observed although the active site was still open (unpublished results), confirming the independent nature of active site closure.

The amount of buried surface area for each monomer in the tetramer of the OXL complex is ~3,380 $Å^2$, comparable to the 3,080 $Å^2$ buried surface area for the NAD^+ binary complex. The collection of residues at the dimer interface in the OXL complex is similar to that in the NAD^+ binary complex[5]. Most of the residues at the dimer interface are involved in similar interactions, and the buried surface area in the dimer is about the same in the two complexes. The slightly larger buried surface area in the OXL complex is due mostly to the tetramer interface. There is a large change in one part of the tetramer interface, involving residues in region 2 (247–250, 481–486 and 541–544) (Fig. 4). This interface includes an additional amino acid, Arg 248, and contributes ~150 $Å^2$ to the extra buried surface area of the OXL complex. Another new residue at the tetramer interface is Lys 22 near the N-terminus that is disordered in the NAD^+ complex. It contributes 85 $Å^2$ of buried surface area to the tetramer interface.

Implications for cooperativity

Structural comparison between the open and closed forms of m-NAD-ME shows that there are three regions that show rigid body movements. If region 2 is used as the reference, two independent rigid body movements are needed to bring the open form to the closed form. The movement of region 1 is related to the change in the tetramer organization, whereas that of region 3 is related to the closure of the active site. These two movements can be uncoupled, however, as observed in the Lu^{3+} complex

Table 1 Summary of crystallographic statistics

Inhibitor / cation	Oxalate / Mn^{++}	Ketomalonate / Mg^{++}	Tartronate / Mg^{++}
Cell parameters	a = 229.0 Å, b = 118.7 Å, c = 113.0 Å, β = 109.6°	a = 229.6 Å, b = 118.6 Å, c = 113.1 Å, β = 109.6°	a = 228.8 Å, b = 117.0 Å, c = 114.3 Å, β = 109.2°
Maximum resolution (Å)	2.2	2.6	2.6
No. of frames (1.5° oscillation)	132	128	100
No. of observations	906,009	688,632	451,060
No. of unique reflections	136,104	84,646	81,974
R_{merge} (%)[1]	7.6	7.6	7.0
Resolution range for refinement	20–2.2 Å	20–2.6 Å	20–2.6 Å
No. of reflections in refinement (F>1σ)	133,588	82,210	80,257
Reflection data completeness (%)	93	94	92
R-factor (%)[2]	20.4	21.8	20.6
R_{free} (%)[3]	26.3	30.1	28.5
R.m.s. deviation			
Bond lengths (Å)	0.008	0.009	0.010
Bond angles (°)	1.3	1.4	1.4
No. of protein residues (atoms)	2,212 (17,472)	2,212 (17,472)	2,212 (17,472)
No. of solvent atoms	959	75	91

[1] $R_{merge} = \Sigma_h \Sigma_i | I_{hi} - \langle I_h \rangle | / \Sigma_h \Sigma_i I_{hi}$.
[2] $R = \Sigma_h | F_h^o - F_h^c | / \Sigma_h F_h^o$.
[3] 7.5% of reflections.

(unpublished data). Residues at the hinges between regions 2 and 3 (279–283 and 465–467) are fairly conserved among the malic enzymes. It may be expected that most malic enzymes could undergo the open-closed transition at the active site. This is likely the mechanism for substrate entry and product release as the active site is completely shielded from the solvent in the closed form. The current structure also suggests that closure of the active site is triggered and stabilized by the binding of the substrate/inhibitors. These are anchored to region 2 *via* the metal ion and other residues but also have interactions with residues in region 3, including, for example, the contributions from the O1B atom of oxalate, from the side chain of Arg 165 (Fig. 2*b*) and from a hydrogen bond between the side chain hydroxyls of Thr 113 and Ser 447.

Human m-NAD-ME is unique among the malic enzymes in that it displays cooperativity with respect to the substrate malate and that its activity is controlled allosterically[9]. The movement of region 1, which contributes to the reorganization of the tetramer, may be the mediator of this allosteric behavior. A conformational change in this region in one monomer, presumably induced by substrate binding, could propagate to the other monomers by the observed movement. The trigger could be the conformational change in helix αA6 (Fig. 2*a*), which is in direct contact with residues in region 1 and is also close to the hinge between regions 1 and 2. It remains to be established whether other malic enzyme tetramers can also undergo rearrangements.

Methods

Protein expression, purification and crystallization. The protocols for the expression and purification of human m-NAD-ME have been described[1,23]. Briefly, m-NAD-ME (containing seleno-methionyl residues) was over-expressed in *E. coli* and purified by anion exchange, ATP affinity and gel filtration chromatography. m-NAD-ME containing seleno-methionyl residues have similar catalytic activity as that of the wild type enzyme. Crystals of m-NAD-ME were obtained at 4 °C by the hanging drop vapor diffusion method. The protein was at 8 mg ml^{-1} concentration, in a solution containing 30 mM Tris (pH 7.4), 80 mM KCl, 4 mM DTT, 0.1 mM EDTA, 0.4–1.2 mM NAD^+, 5–10 mM $MgCl_2$ or $MnCl_2$, 5 mM fumarate, and 5 mM of the substrate-analog inhibitor (tartronate, ketomalonate, oxalate, respectively). The reservoir solution contained 100 mM MES (pH 6.5), 6–11% PEG 20000, and 5% (v/v) 2-methyl-2,4-pentanediol (MPD). Crystals appeared within a few days in the shape of thin plates. For cryo-protection, 0.7 μl of ethylene glycol was introduced into the crystallization mother liquor for 30 min for the tartronate complex. For the ketomalonate and oxalate complexes, the crystals were transferred to a solution containing 100 mM MES (pH 6.5), 30% PEG 8000, 5% MPD (v/v), and 5 mM fumarate for 30 min. The crystals were then flash-frozen in liquid propane.

Data Collection. X-ray diffraction data up to 2.2 Å resolution on crystals of the three inhibitor complexes — oxalate, ketomalonate, and tartronate, respectively — were collected on beamline X4A at the Brookhaven National Laboratory. The oscillation range per image was 1.5° and the exposure time was between 3 and 4 min. The diffraction images were recorded on a CCD Quantum 4 detector and processed with the HKL package (Table 1)[24]. The crystals belong to space group C2, with cell parameters of a = 229.0 Å, b = 118.7 Å, c = 113.0 Å, and β = 109.6° for the oxalate complex. There is a tetramer of m-NAD-ME in the asymmetric unit, giving a V_m of about 3.0 $Å^3$ Da^{-1}.

Structure determination and refinement. The structure of the oxalate complex was determined by the molecular replacement method with the program package Replace[25]. The m-NAD-ME tetramer in complex with NAD^+ (ref. 5) was used as the model in the rotation and translation function calculations, which showed clear peaks for the correct solution. The atomic model based on the molecular replacement solution was subjected to rigid body refinement against reflection data between 5 and 4 Å resolution, with the program X-PLOR[26]. Calculated phases based on this atomic model were applied to all observed reflections between 20 and 2.6 Å resolution. Four-fold non-crystallographic symmetry (NCS) averaging was carried out with the program DM in the CCP4 package[27]. The free R factor after NCS averaging was 24.6%. The resulting electron density map was of excellent quality, and revealed that there were many structural differences to the atomic model of the NAD^+ complex. The atomic model was modified to fit the electron density with the program O[28]. The NAD^+ molecule in the active site was clearly visible in the electron density map, so was the ADP moiety of the second NAD^+ molecule. Both were included in the atomic model at the start of the structure refinement. The electron density for the oxalate inhibitor and the Mn^{++} ion was also visible, and they were included starting from the second round of refinement.

Structure refinement of the ME-oxalate complex was carried out with the program X-PLOR[26] using reflections between 20 and 2.2 Å resolution. NCS restraints were used throughout the structure refinement, initially on all the atoms and finally on only the main chain atoms. After the first round of slow cooling refinement, the positions of the Mn^{++} ions were revealed by 13 σ peaks in the difference electron density map. The identification of the cation binding site was also confirmed by a difference electron density map between the Mn–oxalate complex and Mg–ketomalonate complex. The cations and the oxalate inhibitor molecules were included in subsequent cycles of refinement. Solvent molecules were identified from difference electron density map as

peaks that have reasonable hydrogen bonding partners. Despite the presence of 5 mM fumarate in the crystallization solution and the cryo-protection solution, it could not be located in the electron density map.

The structure refinement of the ketomalonate and the tartronate complexes used the oxalate complex as the starting model. The ketomalonate complex was essentially isomorphous with the oxalate complex. The tartronate complex showed significant shifts in the m-NAD-ME monomer orientation and position during the rigid body refinement. The refinement statistics on all three complexes are summarized in Table 1.

Coordinates. The atomic coordinates have been deposited in the Protein Data Bank (accession codes 1DO8, 1EFK and 1EFL).

Acknowledgments

We thank C. Ogata for setting up the beam line, Y. Xu and R. Khayat for help with data collection at NSLS, W. W. Cleland for many helpful discussions, and H. Wu for comments on the manuscript. This work was supported by a grant from the National Science Foundation to L.T.

Received 26 October, 1999; accepted 4 January, 2000.

1. Loeber, G., Infante, A. A., Maurer-Fogy, I., Krystek, E. & Dworkin, M. B. Human NAD+-dependent mitochondrial malic enzyme. *J. Biol. Chem*. **266**, 3016–3021 (1991).
2. Mallick, S., Harris, B. G. & Cook, P. F. Kinetic mechanism of NAD:malic enzyme from *Ascaris suum* in the direction of reductive carboxylation. *J. Biol. Chem.* **266**, 2732–2738 (1991).
3. Chou, W.-Y., Huang, S.-M., Liu, Y. H. & Chang, G.-G. Cloning and expression of pigeon liver cytosolic NADP+-dependent malic enzyme cDNA and some of its abortive mutants. *Arch. Biochem. Biophys.* **310**, 158–166 (1994).
4. Urbauer, J. L., Bradshaw, D. E. & Cleland, W. W. Determination of the kinetic and chemical mechanism of malic enzyme using (2R,3R)-erythro-fluoromalate as a slow alternative substrate. *Biochemistry* **37**, 18026–18031 (1998).
5. Xu, Y. W., Bhargava, G., Wu, H., Loeber, G. & Tong, L. Crystal structure of human mitochondrial NAD(P)+-dependent malic enzyme: a new class of oxidative decarboxylases. *Structure* **7**, 877–889 (1999).
6. Loeber, G., Dworkin, M. B., Infante, A. & Ahorn, H. Characterization of cytosolic malic enzyme in human tumor cells. *FEBS Lett.* **344**, 181–186 (1994).
7. Baggetto, L. G. Deviant energetic metabolism of glycolytic cancer cells. *Biochimie* **74**, 959–974 (1992).
8. McKeehan, W. L. Glycolysis, glutaminolysis and cell proliferation. *Cell Biol. Int. Rep.* **6**, 635–650 (1982).
9. Sauer, L. A. An NAD- and NADP-dependent malic enzyme with regulatory properties. *Biochem. Biophys. Res. Commun.* **50**, 524–531 (1973).
10. Wierenga, R. K., Terpstra, P. & Hol, W. G. J. Prediction of the occurrence of the ADP-binding bab-fold in proteins, using an amino acid sequence fingerprint. *J. Mol. Biol.* **187**, 101–107 (1986).
11. Wei, C.-H., Chou, W.-Y., Huang, S.-M., Lin, C.-C. & Chang, G.-G. Affinity cleavage at the putative metal-binding site of pigeon liver malic enzyme by the Fe2+-ascorbate system. *Biochemistry* **33**, 7931–7936 (1994).
12. Wei, C.-H., Chou, W.-Y. & Chang, G.-G. Identification of Asp258 as the metal coordinate of pigeon liver malic enzyme by site-specific mutagenesis. *Biochemistry* **34**, 7949–7954 (1995).
13. Satterlee, J. & Hsu, R. Y. Duck liver malic enzyme: sequence of a tryptic peptide containing the cysteine residue labeled by the substrate analog bromopyruvate. *Biochim. Biophys. Acta* **1079**, 247–252 (1991).
14. Vernon, C. M. & Hsu, R. Y. Pigeon liver malic enzyme: involvement of an arginyl residue at the binding site for malate and its analogs. *Arch. Biochem. Biophys.* **225**, 296–305 (1983).
15. Rao, S. R., Kamath, B. G. & Bhagwat, A. S. Chemical modification of the functional arginine residue(s) of malic enzyme from *Zea mays*. *Phytochem.* **30**, 431–435 (1991).
16. You, K. S. Stereospecificity for nicotinamide nucleotides in enzymatic and chemical hydride transfer reactions. *CRC Crit. Rev. Biochem.* **17**, 313–451 (1985).
17. Hall, M. D. & Banaszak, L. J. Crystal structure of a ternary complex of *Escherichia coli* malate dehydrogenase citrate and NAD at 1.9 Å resolution. *J. Mol. Biol.* **232**, 213–222 (1993).
18. Hsu, R. Y., Mildvan, A. S., Chang, G.-G. & Fung, C.-H. Mechanism of malic enzyme from pigeon liver. Magnetic resonance and kinetic studies of the role of Mn2+. *J. Biol. Chem.* **251**, 6574–6583 (1976).
19. Tipton, P. A., Quinn, T. P., Peisach, J. & Cook, P. F. Role of the divalent metal ion in the NAD:malic enzyme reaction: An ESEEM determination of the ground state conformation of malate in the E:Mn:malate complex. *Prot. Sci.* **5**, 1648–1654 (1996).
20. Hurley, J. H., Dean, A. M., Koshland, D. E., Jr. & Stroud, R. M. Catalytic mechanism of NADP+-dependent isocitrate dehydrogenase: Implications from the structures of Magnesium-isocitrate and NADP+ complexes. *Biochemistry* **30**, 8671–8678 (1991).
21. Lee, M. E. *et al*. Mutational analysis of the catalytic residue Lysine 230 and Tyrosine 160 in the NADP+-dependent isocitrate dehydrogenase from *Escherichia coli*. *Biochemistry* **34**, 378–384 (1995).
22. Scrutton, N. S., Berry, A. & Perham, R. N. Redesign of the coenzyme specificity of a dehydrogenase by protein engineering. *Nature* **343**, 38–43 (1990).
23. Bhargava, G. *et al*. Preliminary crystallographic studies of human mitochondrial NAD(P)+-dependent malic enzyme. *J. Struct. Biol.* **127**, 72–75 (1999).
24. Otwinowski, Z. & Minor, W. Processing of X-ray diffraction data collected in oscillation mode. *Method Enzymol.* **276**, 307–326 (1997).
25. Tong, L. Replace: A suite of computer programs for molecular-replacement calculations. *J. Appl. Cryst.* **26**, 748–751 (1993).
26. Brunger, A. T. *The X-PLOR manual* (Yale University, New Haven, Connecticut, 1992).
27. Collaborative computational project, Number 4. The CCP4 suite: programs for protein crystallography. *Acta Crystallogr.* **D50**, 760–763 (1994).
28. Jones, T. A., Zou, J. Y., Cowan, S. W. & Kjeldgaard, M. Improved methods for building protein models in electron density maps and the location of errors in these models. *Acta Crystallogr.* **A47**, 110–119 (1991).
29. Carson, M. Ribbon models of macromolecules. *J. Mol. Graphics* **5**, 103–106 (1987).
30. Nicholls, A., Sharp, K. A. & Honig, B. Protein folding and association: insights from the interfacial and thermodynamic properties of hydrocarbons. *Proteins* **11**, 281–296 (1991).